Journal of Controlled Release 368 (2024) 768–779

Contents lists available at ScienceDirect

Journal of Controlled Release

journal homepage: www.elsevier.com/locate/jconrel

STING-activating cyclic dinucleotide-manganese nanoparticles evoke robust immunity against acute myeloid leukemia

Marisa E. Aikins [a,b,1], Xiaoqi Sun [a,b,1], Hannah Dobson [a,b], Xingwu Zhou [a,b], Yao Xu [a,b], Yu Leo Lei [c,d,e], James J. Moon [a,b,e,f,g,*]

[a] Department of Pharmaceutical Sciences, University of Michigan, Ann Arbor, MI 48109, USA
[b] Biointerfaces Institute, University of Michigan, Ann Arbor 48109, USA
[c] Department of Periodontics and Oral Medicine, University of Michigan, Ann Arbor, MI 48109, USA
[d] Department of Otolaryngology – Head and Neck Surgery, University of Michigan, Ann Arbor, MI 48105, USA
[e] Rogel Cancer Center, University of Michigan, Ann Arbor, MI 48109, USA
[f] Department of Biomedical Engineering, University of Michigan, Ann Arbor, MI 48109, USA
[g] Department of Chemical Engineering, University of Michigan, Ann Arbor, MI 48109, USA

ARTICLE INFO

Keywords:
STING agonist
Nanoparticle
Acute myeloid leukemia
Cancer immunotherapy

ABSTRACT

Acute myeloid leukemia (AML) is one of the most common types of leukemia in adults with a 5-year survival rate of 30.5%. These poor patient outcomes are attributed to tumor relapse, stemming from ineffective innate immune activation, T cell tolerance, and a lack of immunological memory. Thus, new strategies are needed to activate innate and effector immune cells and evoke long-term immunity against AML. One approach to address these issues is through Stimulator of Interferon Genes (STING) pathway activation, which produces Type I Interferons (Type I IFN) critical for innate and adaptive immune activation. Here, we report that systemic immunotherapy with a lipid-based nanoparticle platform (CMP) carrying Mn^{2+} and STING agonist *c*-di-AMP (CDA) exhibited robust anti-tumor efficacy in a mouse model of disseminated AML. Moreover, CMP immunotherapy combined with immune checkpoint blockade against cytotoxic T-lymphocyte-associated protein 4 (anti-CTLA-4) elicited robust innate and adaptive immune activation with enhanced cytotoxic potential against AML, leading to extended animal survival after re-challenge with AML. Overall, this CMP combination immunotherapy may be a promising approach against AML and other disseminated cancer.

1. Introduction

Acute myeloid leukemia (AML) is one of the most common types of leukemia in adults, affecting 20,000 people in the United States and resulting in nearly 12,000 deaths [1]. Although AML accounts for about 1% of all cancers, its incidence is increasing [2], and AML patients have a remission rate of ~67% [1] with the 5-year relative survival rate of just 30.5% [3]. These poor patient outcomes can be attributed to tumor relapse. Notably, AML is characterized by an increase in the number of myeloid cells in the bone marrow and an arrest in their maturation, resulting in hematopoietic insufficiency [4]. In other words, AML cells proliferate rapidly in the bone marrow, depleting nutrients necessary for hematopoiesis, resulting in the inability to produce enough healthy blood cells.

One of the major characteristics of AML is that it is a disseminated cancer with immunosuppressive pathways. Recent studies showed that systemic inoculation of AML cells induces T cell tolerance in an antigen-specific manner [5,6]. Mice inoculated intravenously (i.v.) with C1498.SIY, a murine AML model expressing model antigen SIY, generated lower SIY-specific T cell responses than mice inoculated with C1498.SIY subcutaneously (s.c.) [5,6]. This observation indicates the stark difference in immune surveillance between disseminated cancer and solid cancer. Taking this one step further, i.v. inoculation of C1498.SIY cells, followed by s.c. inoculation of C1498.SIY cells resulted in significantly decreased SIY-specific T cell responses, compared with only s.c. inoculation of C1498.SIY cells [5], showing that AML cells actively promoted T cell dysfunction. However, agonistic anti-CD40 antibody, which activates antigen-presenting cells (APCs), reversed T cell tolerance and

* Corresponding author at: Department of Pharmaceutical Sciences, University of Michigan, Ann Arbor, MI 48109, USA.
E-mail address: moonjj@umich.edu (J.J. Moon).
[1] Authors contributed equally.

https://doi.org/10.1016/j.jconrel.2024.03.022
Received 5 November 2023; Received in revised form 2 March 2024; Accepted 14 March 2024
Available online 20 March 2024

extended animal survival [5]. These results demonstrate that T cell tolerance observed in mice inoculated i.v. with C1498.SIY cells was likely regulated by tolerogenic host APCs in the innate immune system. Thus, activation of innate and effector immune cells may offer a potential strategy to elicit strong immune responses against AML.

Current AML therapies do not effectively activate innate immune cells. The standard of care treatments for AML is a chemotherapeutic approach – the "3 + 7" regimen (3 days of daunorubicin +7 days of cytarabine) and allogeneic hematopoietic cell transplantation [7,8]. In addition to these, targeted therapies have gained attention as the pathophysiological molecular subsets of AML have been identified [8]. Some of these experimental therapeutics include hypomethylating agents, fms-like tyrosine kinase 3 (FLT3) inhibitors, IDH inhibitors, TP53 modulator, menin inhibitors, T cell engagers, chimeric antigen receptor (CAR)-T cells, and immune checkpoints blockers (ICBs) [8].

One approach to effectively activate innate immune cells is through activation of the Stimulator of Interferon Genes (STING) pathway. Cyclic GMP-AMP synthase (cGAS) senses damaged double stranded DNA in the cytosol which catalyzes the production of cyclic [G(2′,5′)pA(3′,5′)p] (cGAMP). cGAMP serves as a secondary messenger and binds to the STING adaptor protein, resulting in the production of Type I Interferons (Type IFNs). While Curran, et al. showed that i.v. administration of a proprietary STING agonist, dithio-(R_P, R_P)-[cyclic[A(2′,5′) pA(3′,5′)p]] (ML RR-S2), induced a significant level of Type I IFN-β *in vivo*, this required a high dose of ML RR-S2 at 100 μg, which resulted in only 25% survival rate in a mouse AML model based on C1498.SIY cells expressing an exogenous antigen, SIY [9]. Therefore, there is a strong need for a delivery system that can exert robust anti-tumor efficacy in a murine model of AML.

We previously reported the development of a STING-activating nanoparticle, termed CMP, and shown their robust efficacy in various models of solid cancer. CMP is a lipid-based nanoparticle loaded with a bacterial STING agonist, cyclic di-AMP (CDA), and manganese ions (Mn^{2+}), which increased Type I IFN activities of STING agonists [10]. Monotherapy with CMP significantly increased STING activation, induced Type I IFNs, reversed immunosuppression in the tumor microenvironment (TME), and exerted strong anti-tumor efficacy in murine models of solid cancer [10]. Here, we have employed the CMP platform as a monotherapy or in combination with ICB to activate innate immune cells and effector T cells in an aggressive model of disseminated C1498 AML [11,12]. Given the ability of systemic AML to induce T cell tolerance [5], we sought to overcome this challenge through STING activation and ICB employment. We report that CMP i.v. therapy led to the accumulation of CMP in the lymphoid tissues and bone marrow, increased Type I IFN production, decreased immunosuppressive cytokines, and induced robust innate and effector T cell responses, while inhibiting the growth of systemic C1498 AML. Furthermore, CMP plus anti-CTLA-4 ICB combination therapy promoted a stronger cytotoxic response and increased immunological memory against C1498 AML.

2. Results and discussion

2.1. Study design

The main objective of our work was to develop an effective immunotherapy against AML and examine its anti-tumor effects. We have previously shown that CMP is a metalloimmunotherapy based on coordination of Mn^{2+} and CDA STING agonist that elicits robust anti-tumor immunity after local or systemic administration [10]. CMP significantly increased STING activation, which was augmented by Mn^{2+}, aptly activated innate immune cell populations, and reversed immunosuppression in murine models of solid cancer. Given the disparity in innate immune activation between AML induced by s.c. and i.v. inoculation of AML cells [6], here we sought to test our hypothesis that systemic administration of CMP would effectively activate innate immunity through increased maturation and activation of DCs and macrophages, and subsequently reverse T cell tolerance against AML tumor cells, leading to induction of anti-AML immunity and therapeutic efficacy against systemically disseminated AML (Fig. 1). Moreover, we evaluated whether innate immune activation, cellular immune activation (T cell responses), and anti-tumor efficacy of CMP against AML can be further improved in combination with anti-CTLA-4, a widely used ICB against AML in clinic [13].

2.2. Synthesis and characterization of CMP

We synthesized CMPs loaded with CDA STING agonist and Mn^{2+} (Fig. 2a). Briefly, $MnCl_2$ solution was added to CDA solution to form CDA-Mn coordinating polymers. CDA—Mn^{2+} interaction was unstable under physiological conditions in phosphate-buffered saline (PBS) and thus, was stabilized with a histidine-tagged lipid which was used as an additional coordination ligand. Dioleoyl-sn-glycero-3-phosphoethanolamine-N-(histidine)11 (DOPE-H11) was synthesized by reacting dioleoyl-sn-glycero-3-phosphoethanolamine-N-(succinimidyloxy-glutaryl) (DOPE-NHS) and H11. DOPE-H11 promoted the formation of a hydrophobic core that could then be coated with an additional layer for aqueous suspension. The resulting CDA-Mn-DOPE-H11 hydrophobic core was then resuspended in a solution containing 1,2-dioleoyl-sn-glycero-3-phosphocholine (DOPC): cholesterol: 1,2-distearoyl-sn-glycero-3-phosphoethanolamine (DSPE)-PEG5000 (in a molar ratio of 4:1:1). After dialysis, the resulting CMPs were analyzed by dynamic light scattering (DLS). CMPs exhibited a hydrodynamic diameter of 125 ± 52 nm, a polydispersity index (PDI) of 0.11, and a slightly positive surface charge of 19.2 ± 2.5 mV (Fig. 2b-c). Transmission electron microscopy (TEM) image of CMP exhibited a spherical particle morphology with a homogenous particle size (**Supplementary Fig. 1a**). The loading efficiency of CDA in CMPs was ~40% as quantified by UV absorbance and Ultra Performance Liquid Chromatography (UPLC, **Supplementary Fig. 1b**). The loading efficiency of Mn^{2+} in CMPs was ~25% as measured by inductively coupled plasma-mass spectrometry (ICP-MS) and thermogravimetric analysis. Release of CDA from CMP reached 55% after 24 h of incubation in PBS (Fig. 2d).

2.3. CMP biodistribution in AML TME

We next examined the biodistribution of CMP in AML-bearing mice (Fig. 3). C57BL/6 mice were inoculated i.v. with 7.5×10^5 C1498 AML tumor cells, and 2 days later, the mice were injected i.v. with CDA/cGAMP-Cy5 in either soluble or CMP form. After 24 h, the animals were euthanized for *ex vivo* imaging of major organs and lymphoid tissues (Fig. 3a-e). The organs assessed were lung, spleen, liver, heart, kidneys, inguinal LNs, and bone marrow. Within 24 h of i.v. administration, free CDA/cGAMP-Cy5 solution was rapidly cleared from the body, with minimal accumulation remaining in the liver and kidneys. In contrast, we observed significantly increased accumulation of $CMP_{CDA/cGAMP\text{-}Cy5}$ in various organs. Importantly, lymphoid tissues, which is considered the TME in AML [14], exhibited robust accumulation of $CMP_{CDA/cGAMP\text{-}Cy5}$. The fluorescence signal of $CMP_{CDA/cGAMP\text{-}Cy5}$ showed an increase of 51-fold, 18-fold, and 12-fold in the spleen, bone marrow, and inguinal LNs, respectively, compared with that of soluble CDA/cGAMP-Cy5 (Fig. 3c-e). Taken together, these results indicate that CMP significantly increases the accumulation of STING agonist in lymphoid tissues where immune cells and AML cells reside. Given that AML increases immunosuppressive immune populations, escapes innate immune recognition, and expresses immune checkpoint markers [15], direct STING activation in lymphoid tissues where AML cells primarily reside in could potentially make AML cells more susceptible to immune cytotoxicity.

2.4. Systemic immune activation

Having shown biodistribution of CMP, we evaluated pro-inflammatory cytokines and chemokines produced in C57BL/6 mice

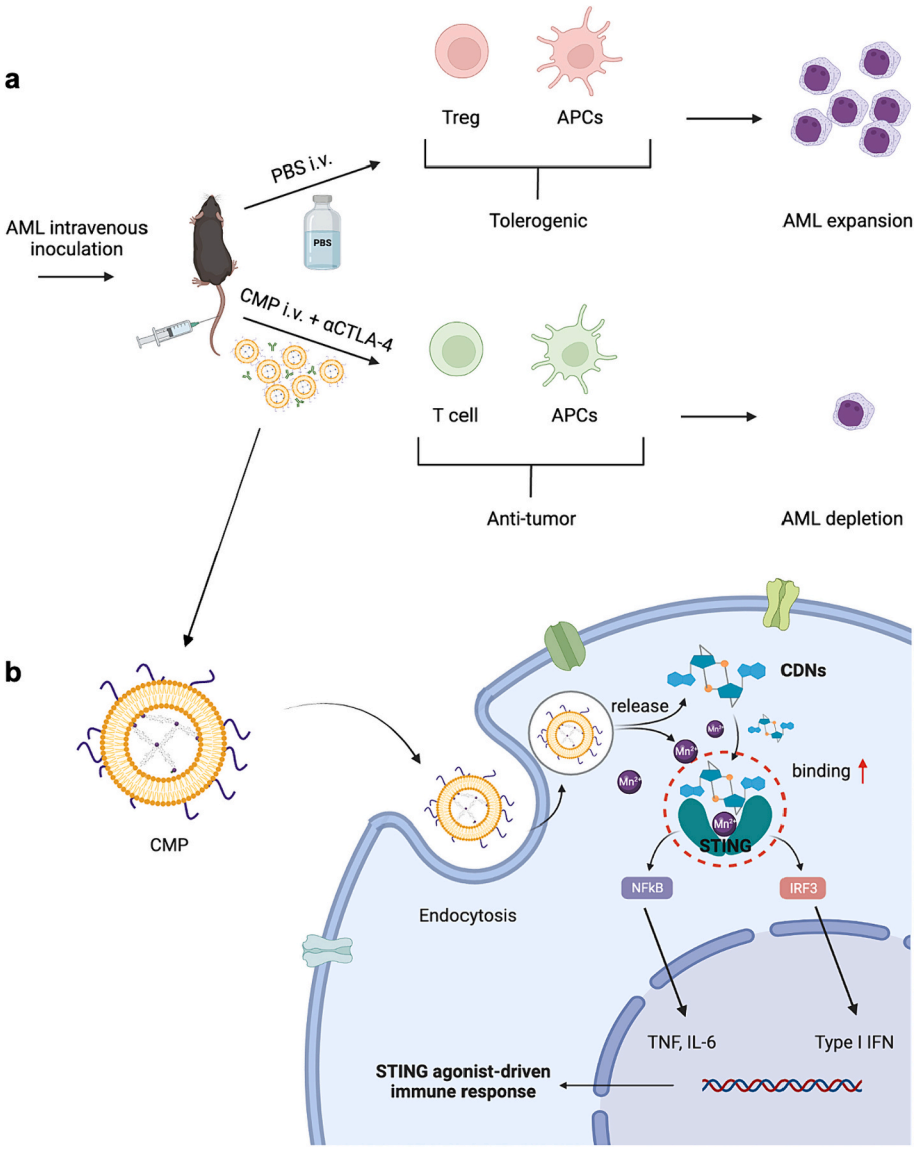

Fig. 1. Schematic illustration of CMP combination immunotherapy against AML. a) Top: i.v. administration of AML leads to tolerogenic immune cells and AML expansion. Bottom: CMP therapy given i.v. leads to an anti-tumor immune response and AML depletion. **b)** CMP enhances STING activation through (1) longer circulation time, (2) increased cellular uptake of CDA and Mn^{2+}, and (3) Mn^{2+} boosts CDA-induced STING activation *via* direct activation of cGAS and augment CDA-STING binding affinity, resulting in Type I IFN production and STING agonist-driven immune responses. Created with BioRender.com.

after i.v. administration of CMP *versus* free CDA + Mn^{2+}. Serum collected 24 h after the first injection (day 2) was analyzed for TNF-α, IFN-β, IFN-γ, and CXCL-10 by ELISA. Mice treated with 10 μg CDA plus 10 μg Mn^{2+} (termed CDA) produced very minimal level of TNF-α, IFN-β, IFN-γ, and CXCL-10 after the first injection (Fig. 4a). In sharp contrast, injection with CMP containing the equivalent dose of 10 μg CDA plus 10 μg Mn^{2+} led to 5600-fold, 5-fold, 250-fold, 42-fold higher levels of in TNF-α, IFN-β, IFN-γ, and CXCL-10 in serum, compared with CDA, respectively (Fig. 4a). Moreover, the second injection with CMP led to 4-fold, 65-fold, 4-fold, and 4-fold higher levels of in TNF-α, IFN-β, IFN-γ, and CXCL-10 in serum, compared with CDA, respectively (Fig. 4b). In addition, TGF-β level was significantly decreased for mice injected with CMP, with 2-fold lower level compared with CDA-treated mice (**Supplementary Fig. 2**), suggesting a less immunosuppressive systemic environment after CMP i.v. therapy.

2.5. Therapeutic efficacy of CMP immunotherapy

To evaluate the therapeutic efficacy of CMP against AML, we employed C1498 cells, which is a highly aggressive disseminated AML model originally isolated from a leukemic 10-month-old C57BL/6 (H-2^b) female mouse in 1941 [11]. Systemic inoculation of C1498 cells leads to their accumulation and proliferation in the blood, lymphoid organs (*e.g.*, lymph nodes and bone marrow), and non-lymphoid organs (*e.g.*, the liver, lungs, ovaries, and kidneys) with a median tumor doubling time of 1.3 days [12]. In our study, we transduced luciferase into C1498 cells for IVIS-based *in vivo* imaging of tumor burden. Specifically, C57BL/6 mice were inoculated i.v. with 7.5 × 10^5 luciferase-expressing C1498 tumor cells on day 0 and treated by i.v. administration with 10 μg CDA plus 10 μg Mn^{2+} either in a free form (CDA) or in CMP on days 2, 9, 16, and 23. In a subset of mice, 100 μg of anti-CTLA-4 IgG was administered intraperitoneally (i.p.) on days 1 and 4 after injection of CDA or CMP (Fig. 5a).

The following treatments were tested *in vivo*: anti-CTLA-4 (termed "αCTLA-4"); CDA + Mn (termed "CDA"); CDA + Mn + anti-CTLA-4 (termed "CDA + αCTLA-4"); CMP; and CMP + anti-CTLA-4 (termed "CMP + αCTLA-4"). Injection with αCTLA-4 or CDA did not slow AML growth, compared with PBS-treated mice (Fig. 5b-c and **Supplementary Fig. 3**).

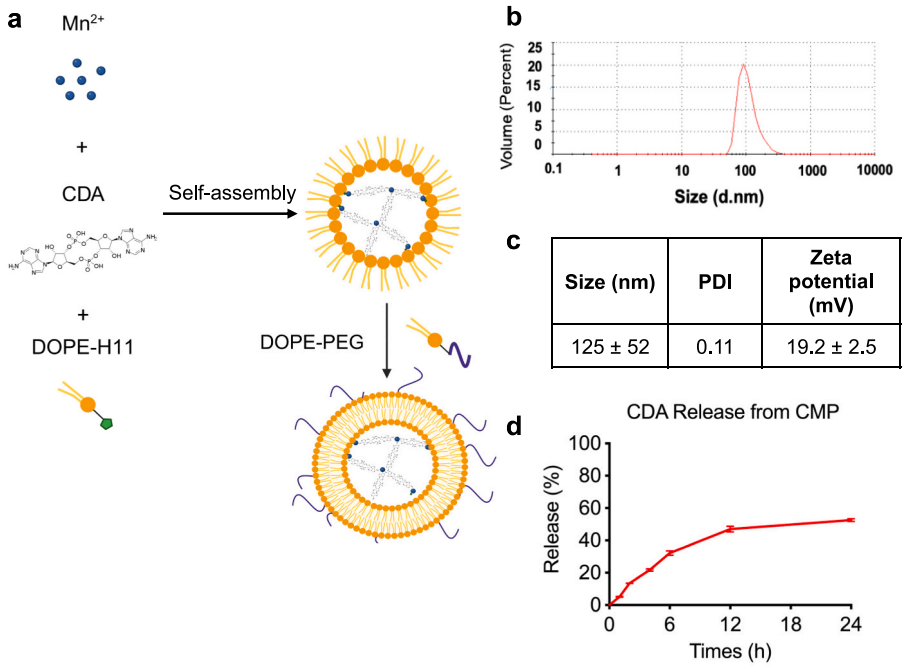

Fig. 2. Synthesis and characterization of CMPs. a) Schematic illustration of CMP synthesis using Mn^{2+}, CDA, and DOPE-Histidine 11 (H11). Created with BioRender.com. **b)** Size distribution of CMP, showing the average diameter of 125 nm. **c)** Zetasizer measurement of CMP, showing an average neutral zeta potential of 19.2 mV and a PDI of 0.11. **d)** Release of CDA from CMP was measured over time in PBS.

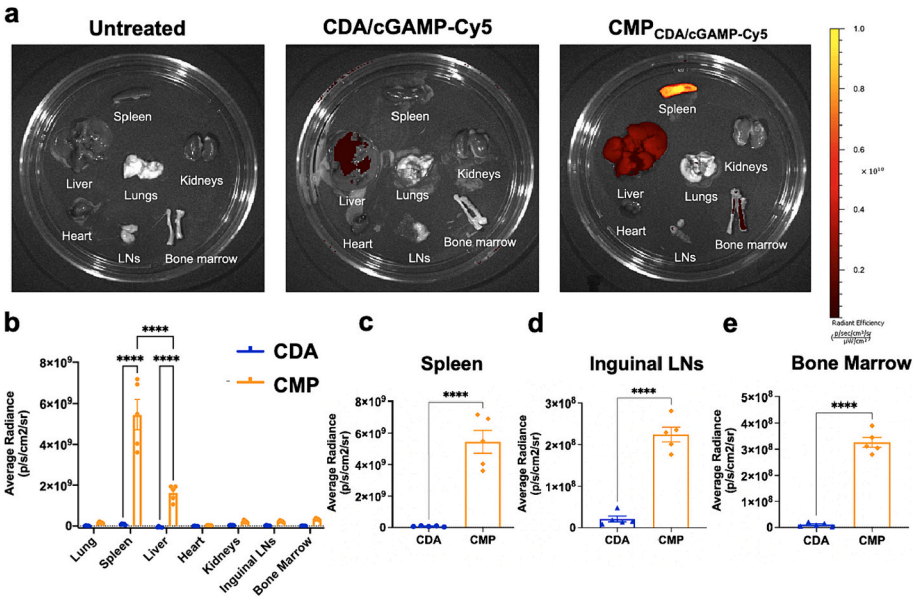

Fig. 3. CMP accumulates in lymphoid tissues. a-e) C57BL/6 mice were inoculated i.v. with 7.5×10^5 C1498 AML tumor cells on day 0 and were injected i.v. on day 2 with CDA/cGAMP-Cy5 in either soluble or CMP form. After 24 h, the major organs and lymphoid tissues were harvested and imaged by *In Vivo* Imaging System (IVIS) for quantification of CDA/cGAMP-Cy5. Shown are **a)** Cy5.5 fluorescence images of the major organs and lymphoid tissues, **b)** quantification of CDA/cGAMP-Cy5 signal in the major organs and lymphoid tissues, **c)** spleen, **d)** inguinal lymph nodes, and **e)** bone marrow. The data show mean ± SEM with $n = 5$/group. ****, $P < 0.0001$.

Unexpectedly, injection with αCTLA-4 alone consistently increased the rate of AML growth, compared with the PBS control. On the other hand, CDA + αCTLA-4 therapy was able to slow tumor growth, compared with PBS-treated mice, but there was no statistically significant difference between the two groups. In stark contrast, CMP monotherapy as well as CMP + αCTLA-4 combo-therapy exerted strong anti-tumor efficacy and significantly reduced the C1498 burden, compared with all other groups (Fig. 5b-c and **Supplementary Fig. 3**). Moreover, CMP as well as CMP + αCTLA-4 therapy significantly extended the animal survival and resulted in approximately 60% survival rate (Fig. 5d), compared with all other treatment groups. There was no statistically significant difference between the CMP monotherapy and the CMP + αCTLA-4 combo-therapy in terms of C1498 AML growth and animal survival.

Taken together, these results demonstrate that CMP-mediated delivery of STING agonist CDA and immune-regulating Mn^{2+} significantly suppressed the growth of systemically disseminated C1498 AML and extended the animal survival, compared with soluble CDA and αCTLA-4 therapy.

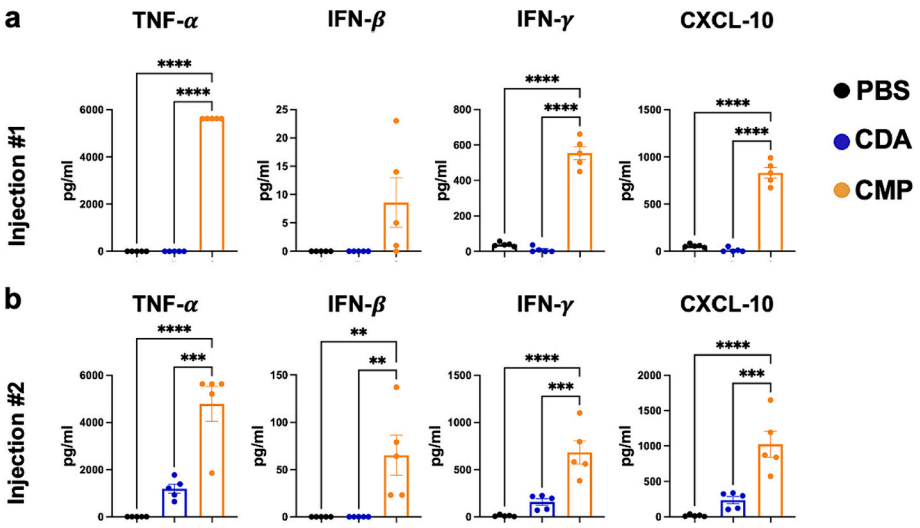

Fig. 4. Impact of CMP injection on serum cytokines. C57BL/6 mice were inoculated i.v. with 7.5×10^5 C1498 AML tumor cells on day 0 and were treated on days 2 and 9 with 10 μg CDA plus 10 μg Mn^{2+} either in a free form (CDA) or in CMP. Serum concentrations of TNF-α, IFN-β, IFN-γ, and CXCL-10 were measured 6 h after each injection on day 2 **a)** and day 9 **b)**.

2.6. Re-challenge of CMP-treated mice

Having shown the robust efficacy of CMP during the primary AML treatment, we evaluated the potential of CMP monotherapy or CMP + αCTLA-4 combo-therapy against AML tumor relapse. To assess this, we treated C1498 AML-bearing mice as shown in Fig. 5a, and on day 40, the remaining survivors were re-challenged by i.v. administration of 7.5×10^5 C1498 cells (Fig. 6a). At this time point, all mice treated with PBS, αCTLA-4, CDA, and CDA + αCTLA-4 had been euthanized, leaving only a subset of mice from CMP monotherapy or CMP + αCTLA-4 combo-therapy. Rather than re-challenging mice that were completely free of AML burden, we re-challenged any mouse remaining at day 40, all of which had minimal AML burden with an average radiance $<1 \times 10^6$ photons/s/cm^2/sr. Notably, 67% of mice previously treated with CMP + αCTLA-4 survived through day 40 ($P < 0.05$, compared with naïve mice, Fig. 6b), compared with 50% survival rate of mice previously treated with CMP monotherapy. Interestingly, a fraction of the mice in both groups that became moribund and needed to be euthanized had low AML burden (Fig. 6c). Because AML is systemic, it can negatively affect any organ or organ system in the body. It is possible that although a low AML burden was observed, latent organ damage from the initial inoculation could be responsible for the moribund state.

Taken together, these results show that mice treated with CMP + αCTLA-4 were able to eliminate AML and efficiently resist AML re-challenge, indicating establishment of immunological memory. However, it does not give a clear mechanism why the addition of αCTLA-4 improved efficacy. We therefore evaluated immune populations in the lymphoid tissues and TME next.

2.7. Immune modulation of lymphoid tissues

Uncontrolled AML systemic growth can result from improper innate immune activation and T cell tolerance [5]. Using CMP, we compensate for this by systemically administering STING agonists in a lipid-based nanoparticle, which is readily taken up by innate immune cells [10], leading to their activation as well as effector T cell activation in lymphoid tissues. Unlike solid cancers where malignant cells form a tumor in a specific location, malignant AML cells are systemic, with tumor accumulation in many compartments, including lymphoid tissues and bone marrow which are considered the major TME in AML [14]. Therefore, we sought to delineate the changes in the spleen and bone marrow after CMP treatment. We treated C1498 AML tumor-bearing mice with 10 μg CDA plus 10 μg Mn^{2+} either in a free form (CDA) or in CMP with or without anti-CTLA-4 IgG as shown in Fig. 5a, followed by immunological analysis of innate immune cells (dendritic cells, macrophages, neutrophils, and monocytes) and effector T cell populations ($CD8^+$ T cells and $CD4^+$ T cells) on day 20 with flow cytometry.

In the spleen, we observed similar levels of $CD11c^+MHC\text{-}II^+$ DCs and total $F4/80^+$ macrophages across all groups (Fig. 7a, **Supplementary Fig. 4**). However, among total $F4/80^+$ macrophages, CMP + αCTLA-4 treatment increased the frequency of $F4/80^+CD206^-$ M1-like macrophages while decreasing the frequency of $F4/80^+CD206^+$ M2-like macrophages, compared with PBS, αCTLA-4, and CDA + αCTLA-4 groups (Fig. 7a). The ratio of M1-like macrophages to M2-like macrophages for the CMP + αCTLA-4 group was 5-fold, 6-fold, 4-fold, and 5-fold higher, compared with PBS, αCTLA-4, CDA, and CDA + αCTLA-4 groups. Both CMP and CMP + αCTLA-4 groups significantly increased the frequency of neutrophils and monocytes in spleen, compared with PBS, CDA, and CDA + αCTLA-4 groups (Fig. 7a). Intratumoral STING activation has been reported to enhance migration of neutrophils to solid tumors and induce neutrophil-mediated T cell activation in tumor-draining LNs [16]. While the role of neutrophils in AML is not well explored, neutrophils may still provide an anti-tumor effect on a systemic level against AML. Monocytes, on the other hand, represent effector immune cells equipped with chemokine receptors and pathogen recognition receptors that mediate migration from blood to tissues in cancer and infection [17] and differentiate into inflammatory DCs or macrophages [17], thus potentially contributing to anti-AML effects.

Next, we determined if the increases in pro-inflammatory innate immune cell populations led to differences in T cell populations in the spleen (Fig. 7b, **Supplementary Fig. 4**). Total $CD8^+$ T cells showed no significant differences across all groups, but effector subpopulations did. Effector memory T cells (Tem) and central memory T cells (Tcm) T cells are critical for immunological memory, with Tcm producing pro-inflammatory cytokines and Tem producing cytotoxic molecules in addition to pro-inflammatory cytokines [18–20]. For both $CD8^+$ T cells and $CD4^+$ T cells, Tem cells showed significant increases for the CMP or CMP + αCTLA-4 groups. Mice injected with CMP + αCTLA-4 had significant increases in the frequency of $CD8^+CD44^{hi}CD62L^-$ Tem cells by 2-fold, 4-fold, and 6-fold in the spleen, compared with αCTLA-4, CDA, and CDA + αCTLA-4 groups, respectively (Fig. 7b). CMP monotheratpy also significantly increased the frequency of $CD8^+CD44^{hi}CD62L^-$ Tem cells by 3-fold and 5-fold, compared with CDA and CDA + αCTLA-4 groups, respectively. Total $CD4^+$ T cells decreased after injection with

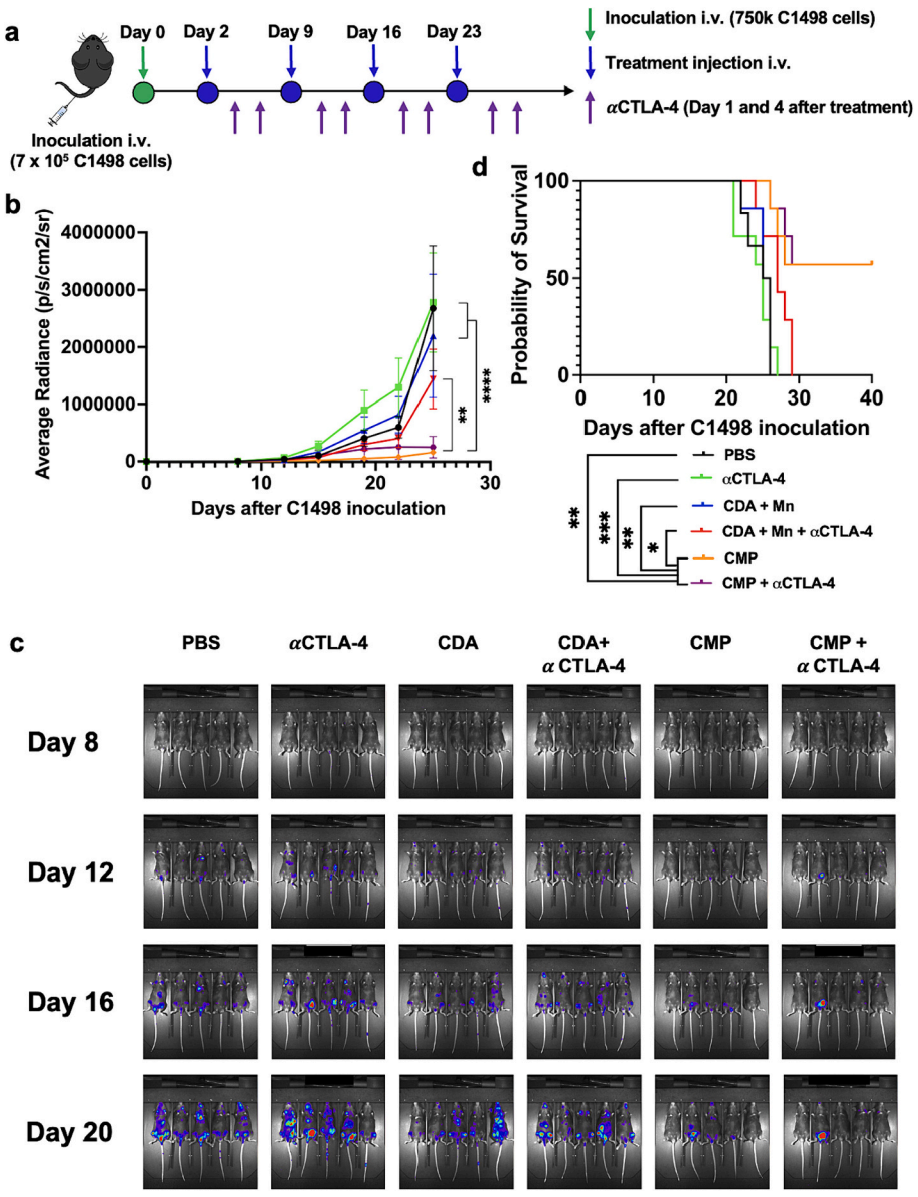

Fig. 5. Therapeutic efficacy of CMP therapy in a systemically disseminated C1498 AML model. a) Treatment regimen and study timeline. C57BL/6 mice were inoculated i.v. with 7.5 × 10^5 C1498 cells on day 0 and treated by i.v. administration of 10 μg CDA plus 10 μg Mn^{2+} either in a free form (CDA) or in CMP with or without αCTLA-4 IgG therapy. Shown are **b)** the average C1498 AML tumor burden, **c)** images of mice visualized over time by whole animal IVIS imaging, and **d)** Kaplan-Meier overall survival curves. The data show mean ± SEM with $n = 8$ mice/group. *, $P < 0.05$; **, $P < 0.01$; ***, $P < 0.001$; ****, $P < 0.0001$.

CMP and CMP + αCTLA-4. Both CMP monotherapy and CMP + αCTLA-4 therapy significantly increased the frequency of $CD4^+CD44^{hi}CD62L^-$ Tem cells and $CD4^+CD44^{hi}CD62L^+$ Tcm cells, while also increasing $CD4^+Foxp3^+$ regulatory T cells (Tregs) in spleen, compared with CDA and CDA + αCTLA-4 groups (Fig. 7b, **Supplementary Fig. 6a**).

We additionally performed immune profiling of the bone marrow as a representative site of the AML TME. $CD11c^+$MHC-II^+ DCs had similar levels across all groups (Fig. 7c). CMP and CMP + αCTLA-4 therapy decreased the frequency of total $F4/80^+$ macrophages. Specifically, while the frequency of $F4/80^+CD206^-$ M1-like macrophages were similar across all groups, CMP and CMP + αCTLA-4 therapy significantly decreased the frequency of $F4/80^+CD206^+$ M2-like macrophages, compared with CMP + αCTLA-4 in bone marrow (Fig. 7c); however, the M1:M2 macrophage ratio was similar for all groups. Notably, CMP + αCTLA-4 therapy significantly increased the frequency of neutrophils, compared with PBS and CDA groups, while CMP therapy significantly increased the frequency of neutrophils and monocytes, compared with PBS and CDA groups in bone marrow (Fig. 7c). For $CD8^+$ and $CD4^+$ T cells in bone marrow, we observed similar changes as in spleen (Fig. 7d, **Supplementary Fig. 5**). Both CMP and CMP + αCTLA-4 groups significantly increased the frequency of $CD8^+CD44^{hi}CD62L^-$ Tem cells, while decreasing $CD8^+CD44^{hi}CD62L^+$ Tcm cells in bone marrow, compared with αCTLA-4 group (Fig. 7d). CMP + αCTLA-4 group significantly increased the frequency of $CD4^+CD44^{hi}CD62L^-$ Tem cells, compared with CDA treatment. $CD8^+CD44^{hi}CD62L^+$ Tcm cells were decreased after treatment with CMP or CMP + αCTLA-4 therapy (Fig. 7d). While there was a trend for degreased level of Tregs in bone marrow for the CMP and CMP + αCTLA-4 groups, the difference was not statistically significant (**Supplementary Fig. 6b**).

Taken together, these results indicate that CMP therapy successfully increased pro-inflammatory innate immune populations in lymphoid tissues, leading to increased effector $CD4^+$ and $CD8^+$ T cells. In particular, we observed a trend of minor increases for activated T cell populations and M1:M2 ratio with the addition of αCTLA-4 to CMP

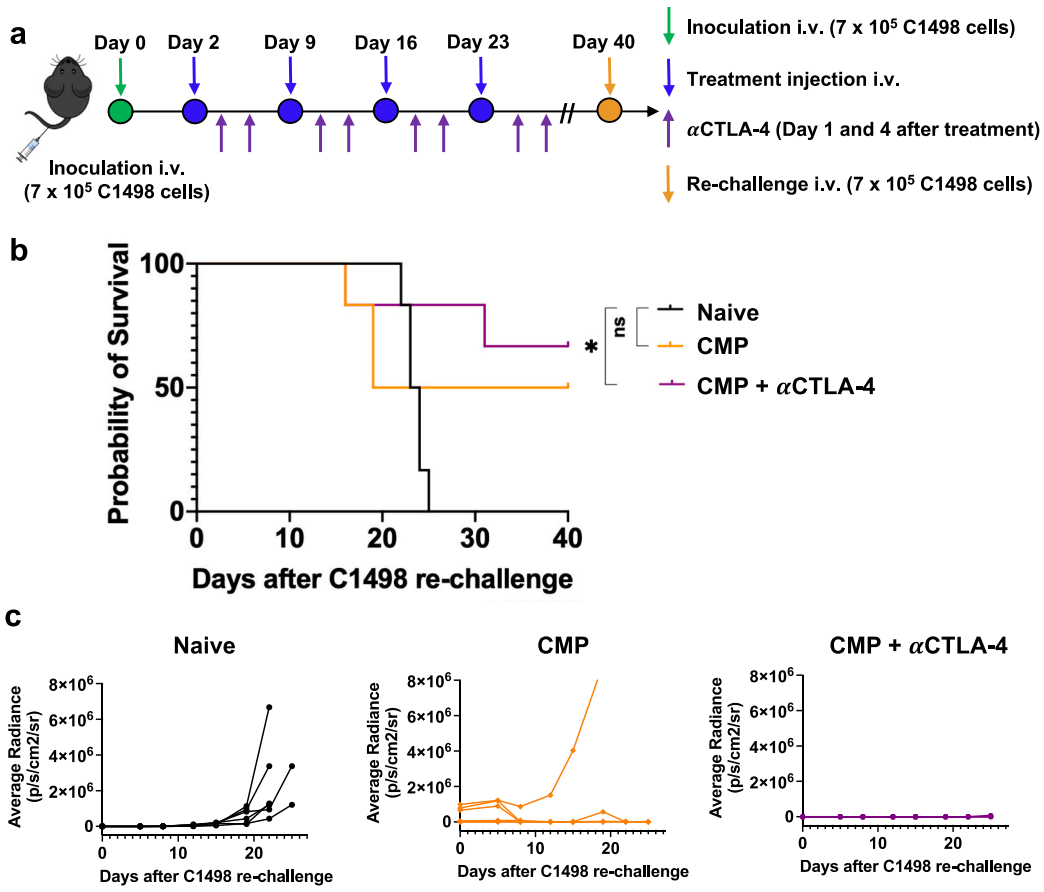

Fig. 6. CMP combination therapy confers immunological memory. a) Treatment regimen and study timeline. C1498 AML-bearing mice were treated as in Fig. 4a. On day 40, the remaining mice were re-challenged by inoculation i.v. with 7.5×10^5 C1498 AML cells, followed by monitoring for tumor growth and animal survival. Shown are **b**) Kaplan-Meier overall survival curves and **c)** individual AML growth curves after the re-challenge. The data show mean ± SEM with $n = 6$ mice/group. *, $P < 0.05$.

treatment. These results corroborate the data from Figs. 5–6, where innate immune and T cell activation likely contributed to the strong *in vivo* efficacy observed.

2.8. Cytotoxic potential of T cells

In addition to evaluating immune populations in the lymphoid tissues, we sought to assess the cytotoxic effect of T cells on C1498 AML tumor cells. We treated C1498 AML tumor-bearing mice with PBS, CMP, or CMP + αCTLA-4. On day 15, $CD8^+$ T cells were isolated from the spleen of mice and activated *ex vivo* with anti-CD3/CD28 for 5 h, followed by incubation with IFN-γ pre-treated C1498 AML cells and quantification of tumor cell lysis after 24 h. Activated $CD8^+$ T cells from spleen of CMP as well as CMP + αCTLA-4 group exhibited efficient lysis of target C1498 AML cells, with a significantly higher rate of killing for the CMP + αCTLA-4 group (Fig. 8a). To understand the impact of CMP mono-therapy and CMP + αCTLA-4 combo-therapy on functionality of T cells, splenocytes isolated on day 15 were activated with anti-CD3/CD28 for 5 h, followed by analysis of cytokines and cytotoxic molecules (Fig. 8b-j). While the total $CD8^+$ T cells for CMP and CMP + αCTLA-4 were decreased in this *ex vivo* set-up (Fig. 8b), activated $CD8^+CD44^{hi}$ T cells were significantly increased for both CMP and CMP + αCTLA-4 groups, compared with PBS (Fig. 8c). Compared with PBS group, $CD8^+CD44^{hi}$ T cells in both CMP and CMP + αCTLA-4 groups significantly increased the expression of Granzyme B (Fig. 8d) with a trend for an increased expression of perforin (Fig. 8e). $CD8^+$ T cells in both CMP and CMP + αCTLA-4 groups showed an increased expression of IFN-γ^+ and IFN-γ^+Granzyme B^+ (Fig. 8f, g). While we did not observe a significant difference between CMP and CMP + αCTLA-4 groups, there was a trend for increased expression of Granzyme B^+ and IFN-γ^+Granzyme B^+ among $CD8^+$ T cells in the CMP + αCTLA-4 group (Fig. 8e, g). In addition, both CMP and CMP + αCTLA-4 groups had significantly increased frequency of activated $CD4^+CD44^{hi}$ T cells with robust IFN-γ expression, compared with the PBS group (Fig. 8h-j). Taken together, these data indicate that CMP treatment induced IFN-γ and Granzyme B-expressing T cells capable of killing AML tumor cells and that the addition of αCTLA-4 therapy amplified $CD8^+$ T cell-mediated killing of AML tumor cells.

3. Conclusion

In this study, we report a novel and powerful immunotherapeutic strategy to target AML. We utilized CMP, a lipid-based nanoparticle consisting of a manganese and CDA STING agonist coordinating polymer. We evaluated the therapeutic efficacy of CMP in the highly aggressive C1498 AML model and examined cytokine production, immune cell populations in lymphoid tissues, and animal survival in a re-challenge model. We have demonstrated that (i) systemic immunotherapy with CMP elicited robust anti-AML efficacy, (ii) CMP accumulated in lymphoid tissues, (iii) CMP activated innate immune cells and effector $CD4^+$ and $CD8^+$ T cell populations in lymphoid tissues, (iv) αCTLA-4 IgG therapy in combination with CMP significantly extended animal survival after re-challenge, and (v) αCTLA-4 therapy increased the cytotoxic potential of $CD8^+$ T cells.

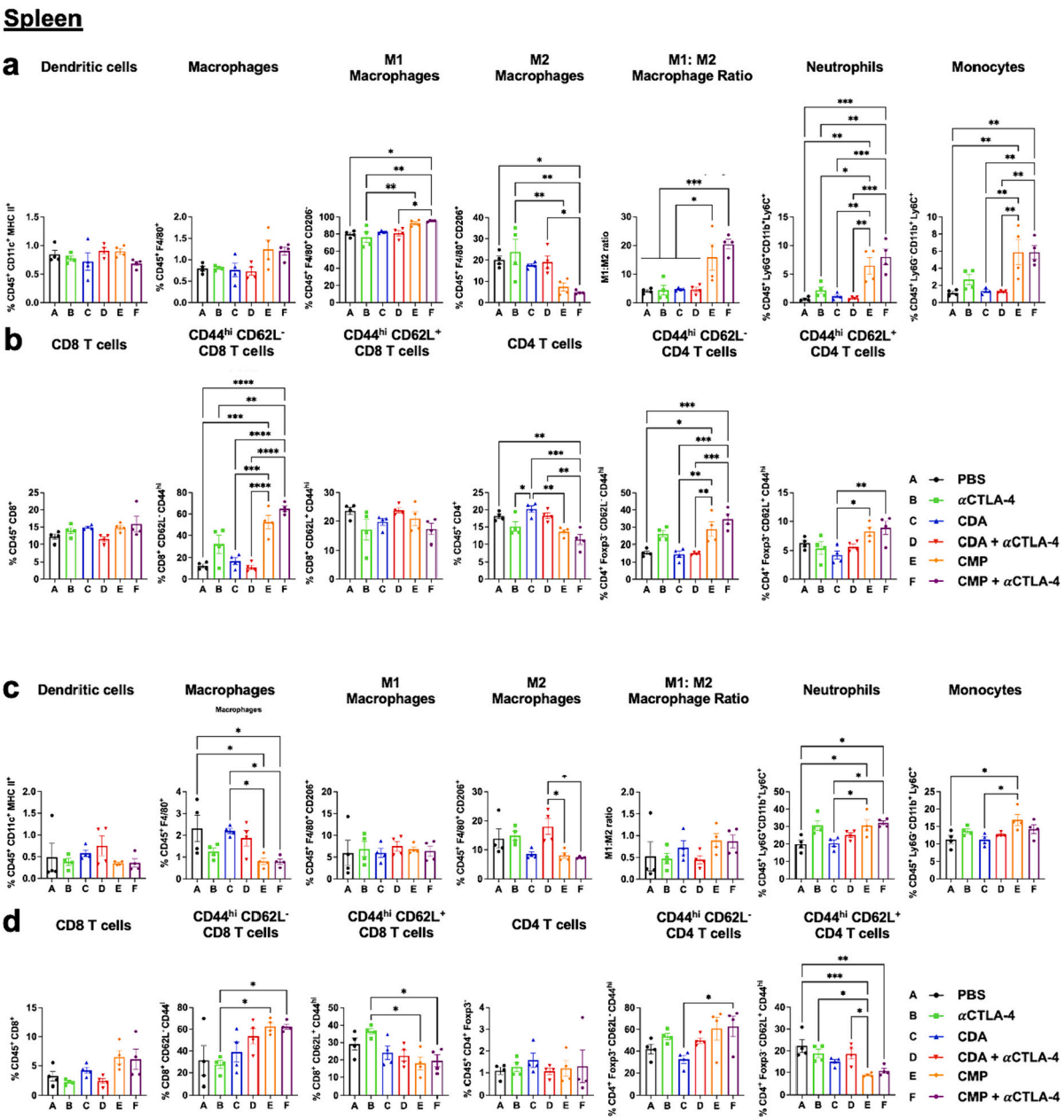

Fig. 7. Impact of CMP injection on lymphocytes in lymphoid tissues. C57BL/6 mice were inoculated i.v. with 7.5×10^5 C1498 AML tumor cells on day 0 and were treated on days 2 and 9 with 10 μg CDA plus 10 μg Mn^{2+} either in a free form (CDA) or in CMP with or without αCTLA-4 IgG therapy. On day 15, cells from spleen (**a-b**) and bone marrow (**c-d**) were stained with antibodies and analyzed by flow cytometry for innate immune cells **(a, c),** $CD8^+$ T cells, and $CD4^+$ T cells **(b, d).** ($n = 4$ mice/group). *, $P < 0.05$; **, $P < 0.01$; ***, $P < 0.001$; ****, $P < 0.0001$.

Despite the exciting results showing the potential of CMP combination immunotherapy against AML, there are still some limitations and room for improvement. For example, the C1498 murine model is a $CD45^+$ myeloid-derived leukemia spontaneous in C57BL/6 mice [11,12], and although it does have some accumulation in the bone marrow, it does not originate there. Because of this, it likely does not alter the hematopoietic stem cell niche into a leukemia niche that becomes permissive of leukemia growth and disrupts normal hematopoiesis as in human AML [21]. Therefore, using a model with spontaneous AML originating in the bone marrow or mimicking it would be ideal. Moreover, because this C1498 cell line has limitations as an AML model, accurate evaluation of the CMP combination therapy with anti-CTLA-4 may require testing in multiple murine AML models that portray key aspects of human AML. Lastly, we have shown that CMP combination therapy with anti-CTLA-4 significantly extends survival after re-challenge and is able to eradicate AML by day 40, which we show is likely due to eliciting more effective cytotoxic responses but may also be due to improved immunological memory. Ultimately, more work needs to be done to better understand the mechanism of action for the CMP combination therapy and the overall safety of CMP.

Overall, the immunotherapeutic approach utilizing CMP in combination with anti-CTLA-4 provides a promising approach to activate the innate immunity and prevent T cell tolerance. The approach outlined here may be broadly applicable to other types of immunosuppressive cancer beyond AML.

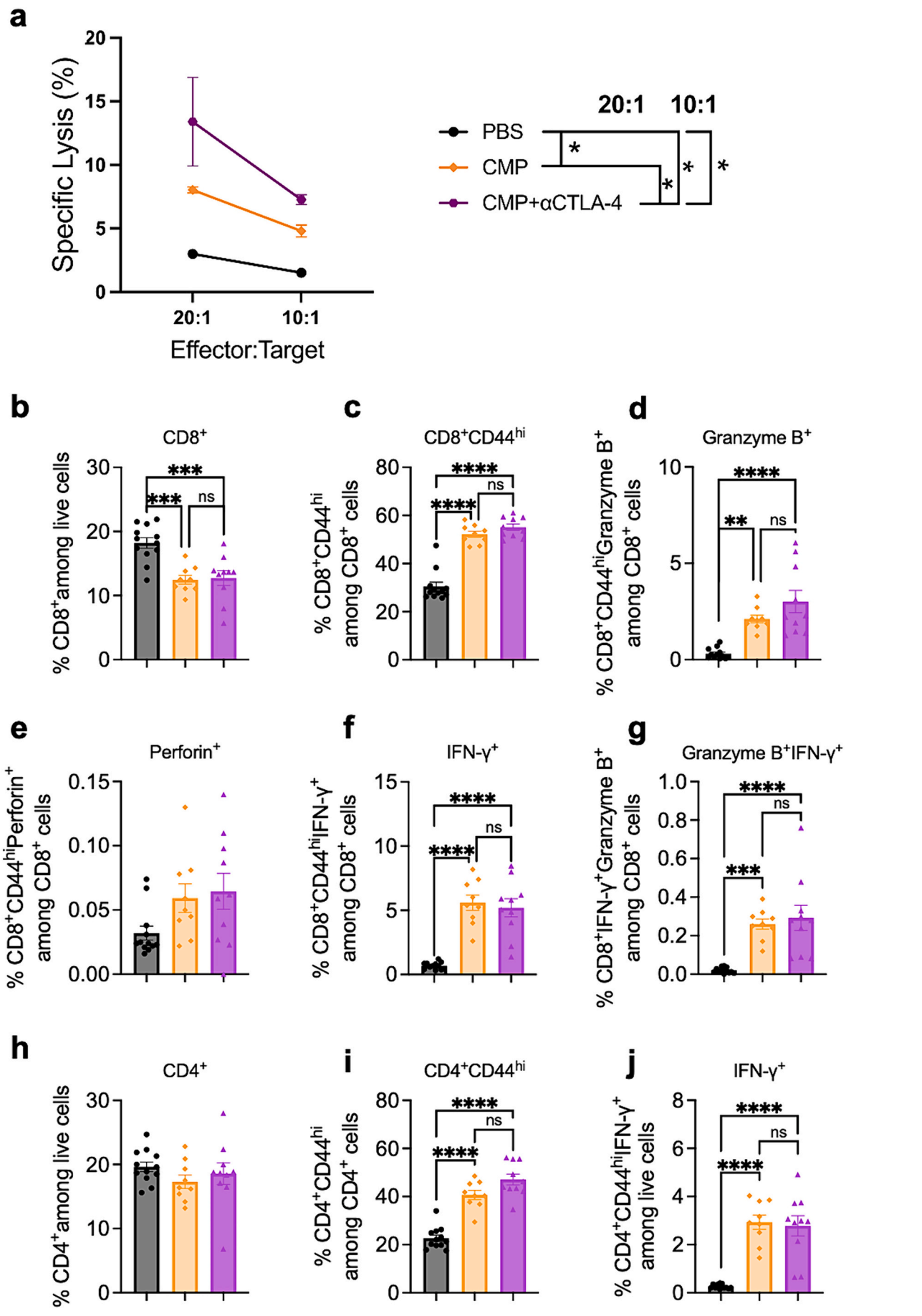

(caption on next page)

Fig. 8. Impact of CMP injection on cytotoxic lymphocyte responses against C1498 AML cells. C57BL/6 mice were inoculated i.v. with 7.5×10^5 C1498 AML tumor cells on day 0 and were treated on days 2 and 9 with CMP with or without αCTLA-4 IgG therapy. **a)** On day 15, $CD8^+$ T cells were isolated from the spleens of mice and activated with anti-CD3/CD28 for 5 h, followed by incubation with IFN-γ-activated C1498 AML cells. After 20 h of incubation, cells were analyzed for tumor-specific lysis. **b-j)** On day 15, splenocytes isolated from the mice were activated with anti-CD3/CD28 for 5 h, followed by flow cytometric analysis for **b)** $CD8^+$ T cells, **c)** $CD8^+CD44^+$ T cells, **d)** $CD8^+CD44^+$Granzyme B^+ T cells, **e)** $CD8^+CD44^+$ $Perforin^+$ T cells, **f)** $CD8^+CD44^+IFN\text{-}\gamma^+$ T cells, **g)** $CD8^+$ $IFN\text{-}\gamma^+$Granzyme B^+ T cells, **h)** $CD4^+$ T cells, **i)** $CD4^+CD44^+$ T cells, and **j)** $CD4^+CD44^+IFN\text{-}\gamma^+$ T cells. (n = 9–12 mice/group). *, $P < 0.05$; **, $P < 0.01$; ***, $P < 0.001$; ****, $P < 0.0001$.

4. Experimental Section

4.1. Study design

The aim of our study was to develop an effective STING agonist-based nanoparticle immunotherapy to target and elicit a comprehensive immune response against AML. We used our previously developed CMP lipid-based particle [10], where STING agonist CDA and Mn^{2+}, known to initiate signaling through binding of the adapter protein STING which is augmented by manganese, can self-assemble into a coordinating polymer, stabilized with an additional coordinating ligand DOPE-11, and finally coated with PEG for aqueous suspension. We characterized the CMPs using dynamic light scattering (DLS), high-performance liquid chromatography (HPLC), and inductively coupled plasma-mass spectrometry (ICP-MS). We then evaluated its efficacy against AML using an i.v. C1498 AML model, a poorly immunogenic and aggressive AML of spontaneous origin [12]. The CMP immunotherapy with and without anti-CTLA-4 was compared to other control groups (n = 8 mice per group). Mice were randomly assigned to treatment groups. Anti-tumor efficacy was assessed by monitoring AML growth curves. We performed immunological assays to measure cytokine and chemokine production, comprehensive immune analysis in lymphoid tissues, and re-challenge.

4.2. Reagents and materials

CDA and CDA/cGAMP-Cy5 are from Invivogen and Biolog, respectively. $MnCl_2$ was purchased from Sigma-Aldrich. dioleoyl-sn-glycero-3-phosphoethanolamine-N-(succinimidyloxy-glutaryl) (DOPE-NHS) and H11 were purchased from NOF America (White Plains, NY) and GenScript (Piscataway, NJ), respectively. 1,2-dioleoyl-sn-glycero-3-phosphocholine (DOPC): and cholesterol–1,2-distearoyl-sn-glycero-3-phosphoethanolamine (DSPE)-PEG5000 (DOPC-cholesterol-DSPE-PEG5000) was purchased from Avanti Polar Lipids (Alabastar, AL). Anti-CTLA-4 was purchased from BioXCell (Lebanon, NH). Cell medium was purchased from Invitrogen (Carlsbad, CA). Female C57BL/6 mice aged 5–7 weeks were purchased from Jackson Laboratories (Bar Harbor, ME). C1498 AML cell line was received from Dr. Haruo Sugiyama at Osaka University Medical School in Osaka, Japan. Dr. Challice Bonifant at Johns Hopkins University of Medicine transduced the C1498 AML cell line with luciferase. The following antibodies used for flow cytometry were obtained from BioLegend: BV421-CD19 (clone HIB19); Pacific Blye-CD8 (clone 53–6.7); BV510-MHC-II (clone M5/114.15.2); BV570-NK1.1 (clone PK136); BV605-CD4 (clone RM4–5); BV650-CD206 (clone C068C2); BV750-CD11c (clone N418); BV785-CD62L (clone MEL-14); FITC-CD45 (clone 30-F11); PerCp-Cy5.5-CD11b (clone M1/70); PE-Foxp3 (clone 150D); PE-Cy5-CD80 (clone 2D10); PE-Cy7-F4/80 (clone BM8); APC-CD3 (clone 17A2); A647-Ki67 (clone 16A8); AF700-CD44 (clone IM7); Live/Dead NIR-Live/Dead.

4.3. Characterization of CMPs

The CMPs were prepared as we previously reported [10] with one difference. Briefly, CDA was dissolved in methanol to produce a 1 mg ml^{-1} solution. $MnCl_2$ was added to the CDA solution at a 10:1 (n/n) ratio under vigorous stirring followed by sonication for 1 min and additional stirring for 1 h at room temperature. The resulting CDN-Mn coordinating polymer was then centrifuged at 20,000g for 10 min to remove excess CDA and Mn^{2+}, followed by washing with methanol. To prepare the stable hydrophobic core, DOPE-H11 was synthesized through a reaction of dioleoyl-sn-glycero-3-phosphoethanolamine-N-(succinimidyloxy-glutaryl) (DOPE-NHS) and H11 (2 equiv.) in *N,N*-dimethylformamide and purified by dialysis using 2 kilodaltons (kD) molecular weight cut-off dialysis tubes. This was characterized by high performance liquid chromatography (HPLC). The mixture containing 1 ml of 1 mg ml^{-1} CDA in methanol, 0.14 ml of 100 mM $MnCl_2$ in methanol, and 2 ml of 1 mg ml^{-1} DOPE-H11 in ethanol was sonicated, vortexed overnight, and centrifuged at 20,000g for 10 min. This CDA-Mn@DOPE hydrophobic core was then resuspended in ethanol containing DOPC-cholesterol-DSPE-PEG5000 (4:1:1) and sonicated. Finally, rather than an ethanol evaporation method, CMPs were dialyzed against 10% sucrose with a and washed with 10% sucrose using centrifugal ultrafiltration (MilliporeSigma Amicon Ultra Centrifugal Filter, 100kD MWCO) at 2800 g for 20 min. CDA loading in CMPs was quantified by UV absorbance at 260 nm and verified by UPLC (Shimadzu). For UPLC method, 10 μL CMP was mixed with 200 μL MeOH to extract the CDA by vortex. After vacuum rotating evaporation at 45C for 0.5 h, 100 μL DI was added to resuspend CDA for UPLC characterization. For UPLC, a reverse phase gradient method with 10 mM ammonium acetate 1% acetic acid/methanol as the mobile phase was used. The flow rate was 200 μl/min, and the retention peak of CDA was around ~4.4 min, as detected at 260 nm. Mn^{2+} loading in CMPs was quantified by inductively coupled plasma-mass spectrometry (ICP-MS; Perkin-Elmer Nexion 2000) and verified by thermogravimetric analysis (Discovery TGA, TA Instruments). The size and surface charge of the CMPs was measured using a Zetasizer Nanoseries Nano-ZS90 (Serial No: Mal1074171). The morphology of CDN–Mn was observed by TEM. All images were acquired on a JEM 1200EX electron microscope (JEOL) equipped with an AMT XR-60 digital camera (Advanced Microscopy Techniques).

4.4. STING agonist immunotherapy treatment groups

The following treatment groups were used in the *in vivo* studies: CDA + Mn^{2+} (CDA), CDA + Mn^{2+} + anti-CTLA-4 (CDA + αCTLA-4), CMP, and CMP + anti-CTLA-4 (CMP + αCTLA-4). For treatment groups containing CDA and Mn^{2+}, the amount of both is 10 μg. For treatment groups containing anti-CTLA-4, the amount is 100 μg.

4.5. Animals

C57BL/6 female mice (6–8 weeks old) were purchased from Jackson Laboratory (Bar Harbor, ME). All animal experiments were conducted in accordance with the approval of the Institutional Animal Care and Use Committee at the University of Michigan (Ann Arbor, MI).

4.6. Biodistribution and safety of CMPs

To analyze the *in vivo* biodistribution of STING agonist, CDA/cGAMP-Cy5 was admixed with CDA (1:10, n/n) to prepare CDA/cGAMP-Cy5@CMP following the same synthesis procedure as used for CMP described above. The loading of CDA/cGAMP-Cy5 was quantified by absorbance at 280 nm. Drug retention in the major organs plus spleen, inguinal lymph nodes, and bone marrow after i.v. injection of CDA/cGAMP-Cy5 in soluble form or in CMP was measured using IVIS. Mice were euthanized 24 h post-injection, and the major organs were excised and imaged by IVIS at 24 h, and the fluorescence signal of CDA/

cGAMP-Cy5 in the tissues was measured accordingly. Drug retention was calculated by normalizing the remaining fluorescence signal of CDA/cGAMP-Cy5 in the tissues at the indicated time point by that of the injected CDA/cGAMP-Cy5 at 0 h. In addition to biodistribution, the weight of mice was also measured every 2 days from day 2 through day 12, which covered the first and second treatment injections.

4.7. In vivo immunotherapy studies

To establish the C1498 AML-bearing tumor mouse model, C57BL/6 mice were inoculated i.v. in the tail vein with 7.5×10^5 cells in HBSS (Hank's balanced salt solution). Mice were randomly divided into six groups ($n = 8$ per group) and received either PBS, CDA, CDA + αCTLA-4, CMP, or CMP + αCTLA-4. Injections of treatments were administered i.v. in the tail vein containing 10 μg of CDA and Mn^{2+}. Injection of 100 μg anti-CTLA-4 ICB was administered intraperitoneally. AML growth was measured every 3–4 days using the *In Vivo* Imaging System (IVIS). Mice were injected with 3 mg luciferin at 15 mg ml^{-1}. Mice were euthanized when the average radiance was 1×10^7 photons/s/cm2/sr, hind limb paralysis occurred, or mice became moribund. Long-term survivors that exhibited complete regression or low-level AML burden were rechallenged 40 days after i.v. inoculation with 7.5×10^5 C1498 cells in the tail vein.

4.8. Re-challenge model

Mice treated with CMP or CMP + αCTLA-4 surviving until Day 40 and with an average radiance $<1 \times 10^6$ photons/s/cm^2/sr were re-challenged with 7.5×10^5 C1498 cells i.v., and AML progression was monitored with IVIS.

4.9. Anti-tumor response induced by CMPs

The ELISA assay was performed on serum from mice injected with either PBS, CDA, CDA + αCTLA-4, CMP, or CMP + αCTLA-4 and was used to measure IFN-β, IFN-γ, TNF-α, TGF-β, and CXCL-10. ELISA was performed by the Cancer Cent Center Immunology Core at University of Michigan, Ann Arbor, MI.

4.10. Immune population analysis

For immune population analyses on spleen, inguinal lymph nodes, bone marrow, and tumor, tissues were processed, washed with fluorescence-activated cell sorting (FACS) buffer, and blocked with CD16/32 antibody. The cells were then stained with the designated antibodies: BV421-CD19 (clone HIB19); Pacific Blye-CD8 (clone 53–6.7); BV510-MHC-II (clone M5/114.15.2); BV570-NK1.1 (clone PK136); BV605-CD4 (clone RM4–5); BV650-CD206 (clone C068C2); BV750-CD11c (clone N418); BV785-CD62L (clone MEL-14); FITC-CD45 (clone 30-F11); PerCp-Cy5.5-CD11b (clone M1/70); PE-Cy5-CD80 (clone 2D10); PE-Cy7-F4/80 (clone BM8); APC-CD3 (clone 17A2); A647-Ki67 (clone 16A8); AF700-CD44 (clone IM7). The cells were washed and stained with live/dead dye for flow cytometric analysis. For Treg analysis, cells were stained with PE-Foxp3 (clone 150D), BV421-CD19 (clone HIB19); BV605-CD4 (clone RM4–5); Pacific Blye-CD8 (clone 53–6.7); FITC-CD45 (clone 30-F11); PerCp-Cy5.5-CD11b (clone M1/70). Cells were then washed and stained with fixable viability dye Live/Dead NIR for flow cytometric analysis.

4.11. Cytokine and CTL analysis

Mice were administered two rounds of CMP injections on Day 2 and 9 +/− anti-CTLA-4 administered on Day 2 and 4 after CMP injection followed by harvesting of spleens on Day 15. Spleens were processed through a 70 μm strainer to produce a single-cell suspension of splenocytes. 2.5×10^6 splenocytes from each mouse were aliquoted for anti-CD3/anti-CD28 activation in a flat bottom 96-well plate that had been previously coated with anti-CD3 (1 μg/ml). Samples were incubated for 5 h at 37C with soluble anti-CD28 (0.5 μg/ml). Brefeldin A (1000×) was added to cultures after 1 h of incubation. After incubation cells were stained with Fixable Live/Dead Dye NIR (Invitrogen) followed by Fc Block, then CD8-BV711, CD4-APC, CD44-BV421. Following the surface stain, cells were fixed and permed for intracellular staining using the eBioscience™ Foxp3 / Transcription Factor Staining Kit according to the manufacturer's instructions. Intracellular antibodies included Granzyme β-FITC, IFN-γ-BV605, and Perforin-PE. From total splenocytes, $CD8^+$ and $CD4^+$ T cells were isolated using the EasySep™ Mouse $CD8^+$ T Cell Isolation Kit (STEMCELL TECHNOLOGIES CA#19853 A) and EasySep™ Mouse CD4+ T Cell Isolation Kit (STEMCELL TECHNOLOGIES CA#19852 A). For the specific lysis analysis, $CD8^+$ T cells were plated in a 96-well plate and co-cultured with IFN- γ pre-treated C1498 AML cells for 20 h. $CD8^+$ T cells were stained with Fixable Live/Dead Dye NIR, CD8-Pac Blue, and CD45-FITC followed by flow cytometric analysis.

4.12. Statistical analysis

Sample sizes were chosen based on preliminary data from pilot experiments and previously published results in the literature. All animal studies were performed after randomization. Data were analyzed by one- or two-way analysis of variance (ANOVA), followed by Bonferroni *post hoc* test for comparison of multiple groups with prism 9.0 (GraphPad Software). Data were normally distributed and variance between groups was similar. P values <0.05 were considered statistically significant. Statistical significance is considered as $^*P < 0.05$, $^{**}P < 0.01$, $^{***}P < 0.001$, $^{****}P < 0.0001$. No samples were excluded from analysis.

CRediT authorship contribution statement

Marisa E. Aikins: Writing – original draft, Investigation, Formal analysis, Conceptualization. **Xiaoqi Sun:** Writing – original draft, Investigation, Conceptualization. **Hannah Dobson:** Investigation. **Xingwu Zhou:** Investigation. **Yao Xu:** Investigation. **Yu Leo Lei:** Investigation. **James J. Moon:** Writing – original draft, Supervision, Funding acquisition, Conceptualization.

Declaration of competing interest

J.J.M. declares financial interests for board membership, as a paid consultant, for research funding, and/or as an equity holder in Saros Therapeutics and EVOQ Therapeutics. The University of Michigan has a financial interest in EVOQ Therapeutics. Y.L.L declares financial interests for board membership and/or as an equity holder in Saros Therapeutics. X.S. is an employee and shareholder in Editas Medicine.

Data availability

Data will be made available on request.

Acknowledgments

This work was supported in part by NIH (R01DE030691, R01DE031951, R01DK125087, R01CA271799, R01NS122536, R01DE026728, R44CA281497), the University of Michigan Rogel Cancer Center Support Grant (P30CA46592), and the Frankel Innovation Initiative at the University of Michigan. We also thank the University of Michigan Flow Cytometry Core, the ULAM (Unit for Laboratory Animal Medicine) and *In Vivo* Animal Core (IVAC).

Appendix A. Supplementary data

Supplementary data to this article can be found online at https://doi.

org/10.1016/j.jconrel.2024.03.022.

References

[1] A.C. Society, Key Statistics for Acute Myeloid Leukemia (AML), 2022.
[2] R.M. Shallis, et al., Epidemiology of acute myeloid leukemia: recent progress and enduring challenges, Blood Rev. 36 (2019) 70–87.
[3] Institute, N.C, Cancer Stat Facts: Leukemia — Acute Myeloid Leukemia (AML), 2022.
[4] H. Dohner, D.J. Weisdorf, C.D. Bloomfield, Acute Myeloid Leukemia, N. Engl. J. Med. 373 (12) (2015) 1136–1152.
[5] X. Chen, D.E. Kline, J. Kline, Peripheral T-cell tolerance in hosts with acute myeloid leukemia, Oncoimmunology 2 (8) (2013) e25445.
[6] L. Zhang, et al., CD40 ligation reverses T cell tolerance in acute myeloid leukemia, J. Clin. Invest. 123 (5) (2013) 1999–2010.
[7] N. Bejanyan, et al., Survival of patients with acute myeloid leukemia relapsing after allogeneic hematopoietic cell transplantation: a center for international blood and marrow transplant research study, Biol. Blood Marrow Transplant. 21 (3) (2015) 454–459.
[8] H. Kantarjian, et al., Acute myeloid leukemia: current progress and future directions, Blood Cancer J. 11 (2) (2021) 41.
[9] E. Curran, et al., STING pathway activation stimulates potent immunity against acute myeloid leukemia, Cell Rep. 15 (11) (2016) 2357–2366.
[10] X. Sun, et al., Amplifying STING activation by cyclic dinucleotide-manganese particles for local and systemic cancer metalloimmunotherapy, Nat. Nanotechnol. 16 (11) (2021) 1260–1270.
[11] A. Mopin, V. Driss, C. Brinster, A detailed protocol for characterizing the murine C1498 cell line and its associated leukemia mouse model, J. Vis. Exp. 116 (2016).
[12] S., U., C1498-Luc-mCherry: A Syngeneic Acute Myeloid Leukemia (AML) Model. 2019, Covance: Covance. https://drugdevelopment.labcorp.com/content/dam/mi-bioresearch/model-spotlights/C1498-LUC-MCHERRY.pdf.
[13] D. Liao, et al., A review of efficacy and safety of checkpoint inhibitor for the treatment of acute myeloid leukemia, Front. Pharmacol. 10 (2019) 609.
[14] A.J. Lamble, E.F. Lind, Targeting the immune microenvironment in acute myeloid leukemia: a focus on T cell immunity, Front. Oncol. 8 (2018) 213.
[15] S. Tettamanti, et al., Catch me if you can: how AML and its niche escape immunotherapy, Leukemia 36 (1) (2022) 13–22.
[16] M.K.A. Nagata, Y. Yajima, S. Yasuda, M. Ohara, K. Ohara, S. Harabuchi, R. Hayashi, H. Funakoshi, J. Ueda, T. Kumai, T. Nagato, K. Oikawa, Y. Harabuchi, C. Esteban, T. Ohkuri, H. Kobayashi, A critical role of STING-triggered tumor-migrating neutrophils for anti-tumor effect of intratumoral cGAMP treatment, Cancer Immunol. Immunother. 70 (8) (2021) 2301–2312.
[17] F. Geissmann, et al., Development of monocytes, macrophages, and dendritic cells, Science 327 (5966) (2010) 656–661.
[18] F. Sallusto, J. Geginat, A. Lanzavecchia, Central memory and effector memory T cell subsets: function, generation, and maintenance, Annu. Rev. Immunol. 22 (2004) 745–763.
[19] L. Lin, et al., Granzyme B secretion by human memory CD4 T cells is less strictly regulated compared to memory CD8 T cells, BMC Immunol. 15 (2014) 36.
[20] W. Ratajczak, et al., Immunological memory cells, Cent Eur J Immunol 43 (2) (2018) 194–203.
[21] L. Behrmann, J. Wellbrock, W. Fiedler, Acute myeloid leukemia and the bone marrow niche-take a closer look, Front. Oncol. 8 (2018) 444.